PCCP

A computational investigation of the electron affinity of CO_3 and the thermodynamic feasibility of $CO_3^-(H_2O)_n$ + ROOH reactions

Christopher D. Cappa and Matthew J. Elrod*

Department of Chemistry, Hope College, Holland, MI 49423 USA. E-mail: elrod@hope.edu; Fax: 1-616-395-7118; Tel: 1-616-395-7629

Received 2nd April 2001, Accepted 4th June 2001
First published as an Advance Article on the web 11th July 2001

The results of electronic structure studies aimed at establishing an accurate theoretical value for the electron affinity of CO_3 are reported. The minimum energy structures for CO_3 and CO_3^- are found to be influenced by the same symmetry breaking effects that have plagued the structure determination of the isoelectronic NO_3^+ and NO_3 species. Although both the planar C_{2v} and D_{3h} minimum energy structures are found for both CO_3 and CO_3^-, and the difference in energy between these two structures is highly dependent on the theoretical method, it is proposed that the true minimum energy structure for each species is the D_{3h} structure, while the C_{2v} structure is believed to be a spurious result that is due to symmetry breaking effects. The electron affinity for CO_3 was calculated with a number of high accuracy methods, resulting in electron affinities ranging between 3.85 to 4.08 eV. These values are significantly higher than some experimental estimates but are in better agreement with more recent experimental results. The thermodynamic feasibility of potential chemical ionization mass spectrometric (CIMS) detection schemes for hydrogen peroxide (H_2O_2) and methyl hydroperoxide (CH_3OOH) using CO_3^- and $CO_3^-(H_2O)$ ionization schemes is also evaluated. An adapted version of G2MS theory was used for calculation of structures and thermodynamic properties of all relevant species for the study of the CIMS schemes. Several thermodynamically feasible $CO_3^-(H_2O)_n$ chemical ionization schemes for the detection of H_2O_2 and CH_3OOH are identified thus indicating that $CO_3^-(H_2O)_n$ CIMS may be a general and selective method for the detection of atmospherically relevant peroxides.

Introduction

The CO_3^- radical anion has been the subject of numerous investigations, in part due to its role as a terminal ion (*i.e.*, relatively stable) in the chemistry of the atmosphere.[1] Chantry *et al.* characterized CO_3^- formed from photoirradiation of $KHCO_3$ using EPR and visible absorption techniques,[2] and Serway and Marshall used EPR techniques to investigate the structure of CO_3^- in calcite crystals.[3] Chantry *et al.* found evidence for a planar C_{2v} structure for CO_3^-, while Serway and Marshall found evidence for both C_{2v} and D_{3h} local CO_3^- geometries, thus suggesting that the crystal environment plays a role in the local structure of CO_3^-. Jacox and Milligan used infrared absorption techniques to investigate CO_3^- in an argon matrix[4] and also found that their results were more consistent with a C_{2v} structure. However the same authors pointed out that NO_3^- also assumes a local C_{2v} geometry in argon matrices, while it is well-established that the bare NO_3^- ion has D_{3h} symmetry. CO_3^- has been studied in the gas phase through photodissociation experiments;[5–7] however there are several excited electronic states present in the spectra which complicate interpretation of the ground state geometry. Early theoretical work using extended Huckel and INDO molecular orbital methods[8] and Hartree–Fock (HF) *ab initio* techniques[9] predicted a planar C_{2v} ground state geometry for CO_3^-. However, more recent work performed by Snodgrass *et al.* using second order Møller–Plesset (MP2) perturbation theory resulted in a D_{3h} ground state geometry.[7] Therefore, it is clear the previous experimental and theoretical work has not resulted in a consensus finding for the structure of CO_3^-.

The CO_3 molecule has been investigated in connection with its potential role in combustion processes. In particular, it has been postulated that CO_3 plays a role in the CO_2-mediated quenching of excited state oxygen atoms.[10] Similar matrix isolation studies on CO_3 as those described above for CO_3^- have concluded that CO_3 also assumes a C_{2v} geometry.[11–13] Early theoretical studies supported the experimentally derived C_{2v} structure,[8,14–20] but more recent correlated treatments have favored the D_{3h} structure.[10,21–23] Therefore, there exists a similar level of uncertainty concerning the structure of the CO_3 as there is concerning the structure of CO_3^-.

Similar issues have been investigated for the NO_3 radical (isoelectronic to CO_3^-), as theoretical methods have produced conflicting results on the relative stability of C_{2v} and D_{3h} structures for fifteen years. Recently, Eisfeld and Morokuma demonstrated that the existence of a C_{2v} minimum for NO_3 is an artifact caused by an inadequate approximation to the electronic Schrodinger equation.[24] In particular, the HF approximation can lead to lower energy "symmetry-broken" solutions that lead to distorted equilibrium geometries. Eisfeld and Morokuma's study confirmed the suspicions of earlier workers in showing that previous theoretical work on NO_3 was influenced by symmetry breaking effects, as these effects dominate HF results, but the effects are masked by MP2 perturbation theory electron correlation treatments (which overestimate the resonance stabilization of the D_{3h} structure), thus leading to the contradictory theoretical results. Miller and Francisco have also recently investigated symmetry breaking effects in the calculated structure for NO_3^+,[25] which is isoelectronic to CO_3.

The CO_3 electron affinity has been measured using a variety of experimental techniques; however these results are spread among a relatively wide range of values (from 2.69–3.48 eV).[6,7,26–31] To our knowledge, there have been no previous computational investigations of the electron affinity of

 DOI: 10.1039/b102981a

CO_3. Therefore, in this study, the ground state structures of CO_3 and CO_3^- are carefully investigated as part of the process in determining the first theoretical value for the electron affinity of CO_3.

CIMS has recently been shown to have much promise for the detection of species such as peroxides that are difficult to measure with optical approaches. Both hydrogen peroxide and methyl hydroperoxide are important atmospheric species by virtue of their role as reservoirs of hydrogen oxide (HO_x) free radical species which play roles in such processes as stratospheric ozone depletion, tropospheric smog formation and acid rain.[32] In particular, Reiner *et al.* have investigated the reaction of $CO_3^-(H_2O)$ with H_2O_2 in a laboratory setting in order to elucidate the identity of ions detected during an aircraft-borne CIMS study of other atmospheric species.[33] Previous work in our laboratory has involved the development of CIMS detection schemes for H_2O_2 and CH_3OOH using $F^-(H_2O)_n$ as the reagent ion.[34] Electronic structure calculations were performed to predict the thermodynamic feasibility of these reactions and experimental studies were performed to verify these predictions. Thermodynamics calculations also supported the feasibility of CIMS detection of CH_3OOH using $H_3O^+(H_2O)_n$ as the reagent ion,[34] and this result has been recently verified experimentally in our laboratory.[35]

As mentioned above, Reiner *et al.* found that $CO_3^-(H_2O)$ can be used to detect H_2O_2 *via* the formation of two stable ionic products through the following proposed reactions:[33]

$$CO_3^-(H_2O) + H_2O_2 \rightarrow CO_3^-(H_2O_2) + H_2O \qquad (1)$$

$$CO_3^-(H_2O) + H_2O_2 \rightarrow O_2^-(H_2O) + CO_2 + H_2O \qquad (2)$$

Aircraft-borne measurement of trace gas species in the lower stratosphere using $CO_3^-(H_2O)$ resulted in detection of ions at 94 and 50 u, which were proposed to correspond to the species $CO_3^-(H_2O_2)$ and $O_2^-(H_2O)$, respectively.[33] An advantage in using $CO_3^-(H_2O)$ reagent ion CIMS over $F^-(H_2O)_n$ reagent ion CIMS is that the $CO_3^-(H_2O)$ ion is naturally prevalent in the atmosphere. Thus, the use of *in situ* $CO_3^-(H_2O)$ CIMS techniques is particularly appealing. In this study, thermodynamic calculations are performed to investigate the thermodynamic feasibility of reactions (1) and (2) as well as to investigate the reactions of hydrogen peroxide with bare CO_3^- and the potential extension of these detection techniques to CH_3OOH in order to investigate the generality of the $CO_3^-(H_2O)_n$ CIMS detection method for peroxides.

Computational methods

CO_3 and CO_3^- structure and energy calculations

HF, MP2 perturbation theory, Becke3-Lee-Yang-Parr (B3LYP) density functional theory (DFT),[36] and coupled cluster (CCSD and CCSD(T))[37,38] calculations were performed using the GAUSSIAN 98 suite of programs.[39] Complete active space self-consistent field (CASSCF)[40] and multi-reference configuration interaction (MRCI)[41] calculations were performed using the MOLPRO 2000 program package.[42] Structure optimization and harmonic frequency calculations were carried out using B3LYP, MP2 and CCSD(T) methods and the split-valence 6-31+G(d) basis set. Additional energy calculations (on MP2/6-31+G(d) optimized structures) were performed with the HF, MP2, CCSD, CCSD(T) and state-averaged CASSCF/MRCI (with Davidson correction) methods using Dunning's correlation consistent valence double- (cc-pVDZ) and triple-zeta basis sets (cc-pVTZ) as well as those basis sets augmented with diffuse functions (aug-cc-pVDZ and aug-cc-VTZ, respectively).[43] HF and MP2 energy calculations were also performed using a valence quadruple-zeta basis (cc-pVQZ) as well as a diffuse function-augmented set (aug-cc-pVQZ).

A full valence space CASSCF calculation is prohibitive for both CO_3 (22 electrons and 16 orbitals) and CO_3^- (23 electrons and 16 orbitals). Therefore, for calculations on ground state D_{3h} CO_3 ($^1A'_1$), a 14 electron, 10 orbital complete active space (CAS) was chosen for use in the CASSCF/MRCI method. The orbitals corresponding to the 1s and 2s orbitals on carbon and oxygen (the lowest 6 a_1 and 2 b_1 orbitals in the Abelian subgroup, C_{2v}) were defined as frozen-core orbitals, and the next highest 3 a_1, 3 b_1, 3 b_2 and 1 a_2 orbitals (comprising the rest of the valence space) were defined as the CAS. Active spaces with an additional a_1, b_1, b_2 or a_2 orbital were investigated, but the reference coefficients indicated there was no significant contribution (<0.05) to the main configuration from excitations to these states. A similar 15 electron, 10 orbital CAS was chosen for calculations on ground state D_{3h} CO_3^- ($^2A'_2$).

The G2 and modified G2MS (described below) model chemistry methods were also used to carry out energy calculations for CO_3 and CO_3^-. In order to calculate standard (1 atm, 298 K) thermodynamic values, vibrational frequencies recovered from MP2/6-31+G(d) calculations were used in conjunction with statistical thermodynamic methods. Electron affinities were calculated from the standard enthalpies of D_{3h} CO_3 and CO_3^-.

Modified G2MS method for chemical ionization reaction energetics

For consideration of the proposed chemical ionization reactions, the energies of the relevant species were calculated using an adapted version of the G2MS compound method,[44] a variation on G2 theory.[45] G2 theory utilizes a series of relatively low-level calculations that are combined in order to determine the equilibrium geometry and total energy. Although usually quite accurate, the G2 method is relatively expensive. The geometry is optimized at the MP2/6-31G(d) level, thus substantially limiting the size of molecules on which calculations can be done. The G2MS method, on the other hand, calculates the molecular geometry at the B3LYP/6-31G(d) level[36] leading to substantial savings in computational resources and allowing for application to systems containing up to ten heavy atoms, much larger than possible with the G2 method.[44] Also, whereas the G2 method includes nine different calculations, the G2MS method only uses five calculations. Most of the G2MS calculations are similar to G2 calculations, however the basis set used for a given electron correlation level is typically slightly smaller for G2MS making G2MS less expensive without much compromising reliability. Additionally, we have adapted the G2MS method such that the geometry was optimized using the B3LYP/6-31G(d,p) level of theory (B3LYP/6-31+G(d,p) for anions). This adaptation allows for slightly more accurate results for the hydrogen-containing species. The vibrational frequencies were obtained from analytical derivatives calculated at this same level of theory and each stationary point was confirmed as a potential energy minimum by inspection of the calculated frequencies. To calculate the overall energy of the optimized structure, a base energy calculation was performed at the CCSD(T)/6-31G(d) level (CCSD(T)/6-31+G(d) for anions). A series of additive corrections (to correct for basis set effects) were then performed in order to simulate a CCSD(T)/6311+G(2df,2p) level calculation. The overall energy expression for the adapted G2MS scheme is defined as

$$\begin{aligned} E(\text{G2MS}) = {} & E[\text{CCSD(T)/6-31G(d)}] \\ & + E[\text{MP2/6-311+G(2df,2p)}] \\ & - E[\text{MP2/6-31G(d)}] + \text{HLC} \qquad (3) \end{aligned}$$

where HLC is an empirically defined correction term with $\text{HLC} = An_\alpha + Bn_\beta$ where n_α and n_β are the number of α and β

electrons, respectively. The constants A and B are defined as 6.06 and 0.19 mH, respectively. For all steps, diffuse basis sets were used for anions. Additionally, the enthalpy and Gibbs energy for each molecule were calculated by addition of the appropriate energy correction term (recovered from statistical thermodynamic calculations as described above for CO_3 and CO_3^-) to the above energy expression.

Validation calculations to establish quantitative accuracy

In order to estimate the quantitative accuracy of our G2MS results, several benchmark calculations were performed: the ionization potential of O_2, electron affinity of NO_2, proton affinity of H_2O, fluoride affinity of HCl and heat of hydration of both O_2^- and CO_3^-. These thermodynamic values were chosen because of the existence of accurate experimental ion thermodynamic data and previous higher-level (G2) computational data for each of the species.

Results and discussion

Geometry optimizations for CO_3 and CO_3^-

Previous theoretical studies of CO_3 and CO_3^- indicated the possibility of two equilibrium structures: a D_{3h} structure and a planar C_{2v} structure with two long C–O bonds and one short C–O bond (2L1S) and a bond angle of less than 120° for the unique angle.[7–10,23] Previous studies of the NO_3 radical (isoelectronic to CO_3^-) have also indicated the possibility of a planar C_{2v} structure with one long C–O bond and two short C–O bonds (1L2S) and a bond angle of greater than 120° for the unique angle.[46] We performed MP2/6-31+G(d) geometry optimizations starting from the D_{3h} and the 2L1S and 1L2S C_{2v} geometries for both CO_3 and CO_3^-. For CO_3^-, potential energy minima were obtained for all three structures (as determined by inspection of the harmonic frequencies). However, the 1L2S energy was found to be significantly higher than the 2L1S energy. Therefore, this structure was not considered further. For CO_3, the 1L2S structure optimized to the D_{3h} geometry, but both the D_{3h} and 2L1S C_{2v} structures were found to be potential energy minima. Similar B3LYP/6-31+G(d) geometry optimizations were performed for CO_3 and CO_3^- starting from the D_{3h} and 2L1S C_{2v} structures. In this case, both the D_{3h} and 2L1S C_{2v} structures were found to be potential energy minima for CO_3, but the 2L1S C_{2v} structure optimized to D_{3h} for CO_3^-. This phenomenon has also been observed for DFT optimizations for the isoelectronic NO_3 radical, but this result was initially attributed to a failure of DFT.[47] We will argue here, as Sherill *et al.* did in the case of NO_3,[48] that this is evidence for a symmetry breaking effect in CO_3^- (*i.e.*, the C_{2v} minimum is an artifact attributable to the choice of the UHF wavefunctions). This point will be discussed further in a subsequent section devoted to symmetry breaking effects.

The minimum energy structures for the D_{3h} and 2L1S C_{2v} geometries of CO_3 and CO_3^- found by each optimization method are reported in Table 1 ($R1$ refers to the unique bond on the C_2 symmetry axis, $R2$ refers to the equivalent bonds, and $A1$ refers to the angle between $R1$ and $R2$). The MP2/6-31+G(d) structures for D_{3h} and C_{2v} CO_3 are in excellent agreement with the nearly identical MP2/6-31G(d) optimizations for both geometries performed by Froese and Goddard (D_{3h}: $R = 1.285$ Å; C_{2v}: $R1 = 1.187$ Å, $R2 = 1.346$ Å, $A1 = 142.7°$).[10] The MP2/6-31+G(d) D_{3h} structure for CO_3^- is also in excellent agreement with the nearly identical MP2/6-311+G(d) optimization performed by Snodgrass *et al.* ($R = 1.280$ Å).[7] We are not aware of any previous theoretical studies of C_{2v} structures for CO_3^- using correlated methods with which we may compare our results. The B3LYP and CCSD(T) structure optimizations do not result in significantly different geometries from those obtained from the MP2 method for either the C_{2v} or D_{3h} structures for CO_3 and CO_3^- (with the exception of the lack of a C_{2v} minimum for CO_3^- using DFT). The harmonic vibrational frequencies obtained by each method are reported in Table 2.

Theoretical method and basis set effects on relative energies of C_{2v} and D_{3h} structures for CO_3 and CO_3^-

The dependence of the relative energies of the C_{2v} and D_{3h} structures for CO_3 and CO_3^- as a function of theoretical method and basis set was investigated by calculating the HF, MP2, CCSD and CCSD(T) energies using Dunning's double-, triple- and quadruple- (for HF and MP2 calculations) zeta basis sets as well as the same basis sets augmented with diffuse functions at the MP2/6-31G+(d) optimized geometries. The results are contained in Table 3. The energy differences between the D_{3h} and C_{2v} structures for CO_3 and CO_3^- as a function of basis set for the different levels of theory are given in Fig. 1 and 2, respectively. This data shows that the D_{3h}

Table 1 Minimum energy structures for CO_3 and CO_3^-

	D_{3h} R /Å	C_{2v} $R1$ /Å	$R2$ /Å	$A1$ /degrees
CO_3 B3LYP/6-31+G(d)	1.2551	1.1795	1.3367	143.5
CO_3 MP2/6-31+G(d)	1.2861	1.1883	1.3469	142.8
CO_3 CCSD(T)/6-31+G(d)	1.2715	1.1884	1.3443	141.8
CO_3^- B3LYP/6-31+G(d)	1.2779	collapses to D_{3h}		
CO_3^- MP2/6-31+G(d)	1.2855	1.2510	1.3050	127.2
CO_3^- CCSD(T)/6-31+G(d)	1.2846	1.2601	1.3010	124.3

Table 2 Harmonic frequencies (in cm^{-1}) for CO_3 and CO_3^-

C_{2v} symmetry	A_1	A_1	A_1	B_1	B_2	B_2
CO_3 MP2/6-31+G(d)	653	1080	2032	655	553	1105
CO_3 B3LYP/6-31+G(d)	695	1127	2073	651	558	943
CO_3^- MP2/6-31+G(d)	521	1085	1675	803	633	2881
CO_3^- B3LYP/6-31+G(d)	collapses to D_{3h}					
D_{3h} symmetry	E'	A_2''	A_1'	E'		
CO_3 MP2/6-31+G(d)	637	703	993	3642		
CO_3 B3LYP/6-31+G(d)	292	751	1142	1532		
CO_3^- MP2/6-31+G(d)	724	791	1074	2616		
CO_3^- B3LYP/6-31+G(d)	376	819	1096	1295		

Table 3 Basis set and level of theory dependence of the energies (in E_h) for CO_3 and CO_3^- using MP2/6-31+G(d) optimized geometries

	cc-pVDZ	aug-cc-pVDZ	cc-pVTZ	aug-cc-pVTZ	cc-pVQZ	aug-cc-pVQZ
CO_3 D_{3h}						
HF	−262.223 14	−263.241 84	−262.296 78	−262.300 69	−262.316 20	−262.317 32
MP2	−263.050 98	−263.109 98	−263.297 64	−263.318 28	−263.380 03	−263.389 12
CCSD	−262.986 78	−263.040 16	−263.217 40	−263.235 52		
CCSD(T)	−263.043 45	−263.102 51	−263.292 11	−263.312 57		
CASSCF/MRCI	−263.757 88	−263.797 10	−262.899 44	−262.910 17		
CO_3 C_{2v}						
HF	−262.326 84	−262.344 88	−262.406 35	−262.409 50	−262.425 28	−262.426 11
MP2	−263.022 00	−263.077 43	−263.272 49	−263.291 88	−263.354 60	−263.363 23
CCSD	−263.019 44	−263.072 01	−263.258 71	−263.276 50		
CCSD(T)	−263.048 04	−263.105 96	−263.303 38	−263.323 35		
CO_3^- D_{3h}						
HF	−262.450 05	−262.493 73	−262.539 31	−262.553 61	−262.564 79	−262.570 33
MP2	−263.138 36	−263.233 99	−263.410 64	−263.446 49	−263.503 56	−263.519 23
CCSD	−263.126 16	−263.216 27	−263.386 40	−263.418 95		
CCSD(T)	−263.152 67	−263.250 53	−263.430 16	−263.466 60		
CASSCF/MRCI	−262.868 32	−262.939 16	−263.031 81	−263.055 94		
CO_3^- C_{2v}						
HF	−262.471 51	−262.510 58	−262.559 22	−262.571 09	−262.583 58	−262.587 81
MP2	−263.126 98	−263.220 41	−263.398 32	−263.433 49	−263.490 89	−263.506 29
CCSD	−263.129 77	−263.218 30	−263.389 92	−263.421 79		
CCSD(T)	−263.152 59	−263.249 03	−263.429 56	−263.465 43		

geometry is predicted to be the minimum energy structure for both CO_3 and CO_3^- at the MP2 level of theory, regardless of the basis set used. This data also shows that the C_{2v} geometry is predicted to be the minimum energy structure for both CO_3 and CO_3^- at the HF and CCSD levels of theory, regardless of the basis set used. The CCSD(T) calculations show that the D_{3h} and C_{2v} structures are roughly isoenergetic for both CO_3 and CO_3^- for all basis sets investigated. Fig. 3 illustrates $\Delta E(D_{3h} - C_{2v})$ explicitly as a function of level of theory for the aug-cc-pVTZ basis set. It is clear that the theoretical methods employed do not produce a definitive result concerning the geometry of the minimum energy structure.

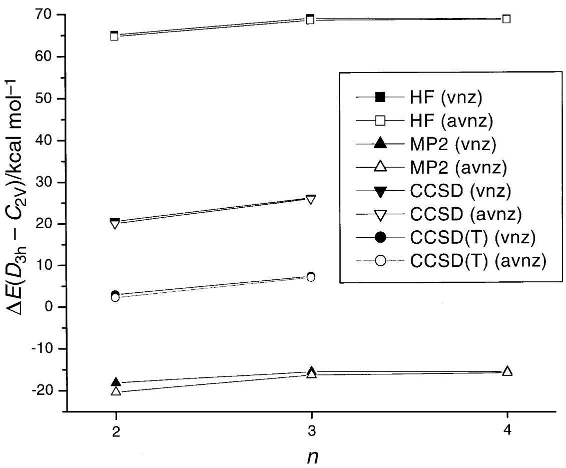

Fig. 1 $CO_3(D_{3h} - C_{2v})$ energy differences determined with several different theoretical methods as function of increasing basis set size (vnz: standard; avnz: augmented correlation consistent basis set).

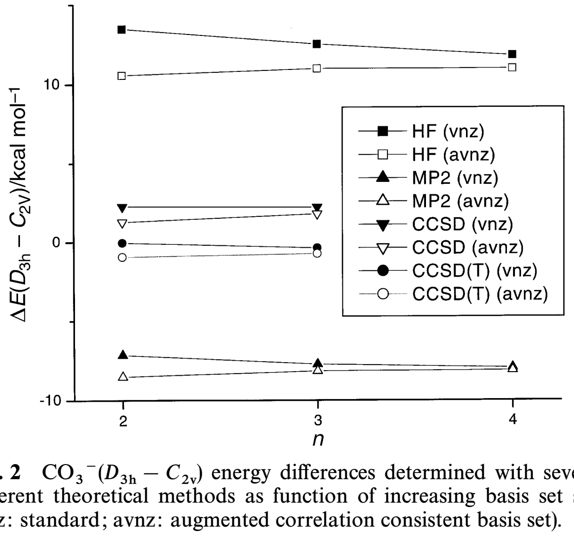

Fig. 2 $CO_3^-(D_{3h} - C_{2v})$ energy differences determined with several different theoretical methods as function of increasing basis set size (vnz: standard; avnz: augmented correlation consistent basis set).

Evidence for symmetry breaking effects in CO_3 and CO_3^-

The careful work of Eisfeld and Morokuma[24] on the structure of NO_3 resulted in the conclusion that previous theoretical findings for a C_{2v} minimum were the result of symmetry breaking effects, and the only true physical minimum for NO_3 is the D_{3h} structure. This result was obtained only with a CASSCF/MRCI approach in which the CAS was carefully chosen to be invariant under the symmetry operations of the D_{3h} point group. In fact, when the almost entirely empty $5a'_1$ orbital was left out of this symmetry-constrained CAS, the calculations again resulted in the spurious C_{2v} minimum. All other theoretical methods lead to the two apparent potential energy C_{2v} and D_{3h} minima. Eisfeld and Morokuma also discussed several indicators of potential symmetry breaking behavior from the results of these other theoretical methods

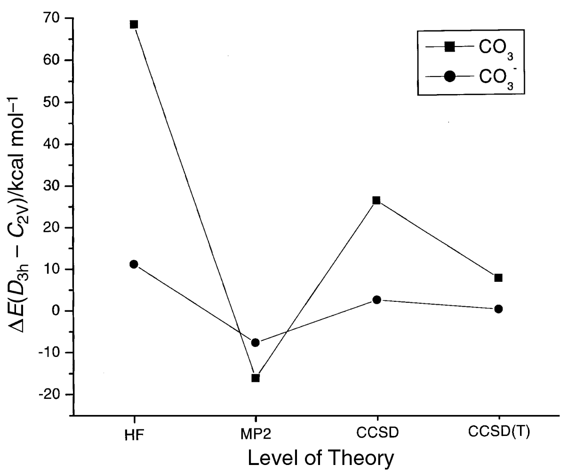

Fig. 3 $(D_{3h} - C_{2v})$ energy differences using the aug-cc-pVTZ basis set as a function of theoretical method.

for NO_3. In particular, they note that the UHF wavefunctions are prone to favor the symmetry breaking C_{2v} structure because of the energy lowering due to orbital localization. Thus, Eisfeld and Morokuma are able to rationalize the result that their UHF calculations place the spurious C_{2v} structure at lower energy than the D_{3h} structure. In contrast, their MP2 calculations indicate a reversed order, with the D_{3h} structure lower in energy. This result is rationalized with the observation that MP2 calculations often overestimate resonance effects which, in the case of NO_3, apparently compensates for the symmetry breaking energy lowering in the UHF wavefunctions. For the coupled cluster methods, CCSD and CCSD(T), Eisfeld and Morokuma find that the C_{2v} and D_{3h} structures are almost isoenergetic, as the coupled cluster method more accurately handles electron correlation (as compared to MP2), and the symmetry breaking energy lowering in the UHF wavefunctions is almost exactly offset by the resonance effect. They also find that Jahn–Teller distortions from a D_{3h} to a C_{2v} geometry (a true physical effect rather the spurious symmetry breaking effect discussed above) are likely not present in NO_3 because the optimized C_{2v} structure is not distorted towards the structure of the $^2B_2$ electronic state, as one would expect from symmetry-based coupling arguments.

Fig. 3 indicates that precisely the same behavior for CO_3 and CO_3^- is observed in this study for similar HF, MP2, CCSD, CCSD(T) calculations as those described by Eisfeld and Morokuma for NO_3: the HF method favors the C_{2v} structure, the MP2 method favors the D_{3h} structure, and the CCSD(T) method indicates the C_{2v} and D_{3h} structures are roughly isoenergetic. Recently, Miller and Francisco[25] reported that symmetry breaking effects are likely present in NO_3^+, which is isoelectronic to CO_3. Therefore, it seems highly likely that symmetry breaking effects are present in the computational results for both CO_3 and CO_3^-. With the additional result that B3LYP geometry optimizations for CO_3^- do not result in a C_{2v} stationary state and that such DFT calculations are expected to be less prone to symmetry breaking effects, it seems likely that the D_{3h} structure is the only true physical minimum for CO_3^-. As noted in the introduction, there is some experimental evidence for a C_{2v} structure for CO_3^- from IR matrix studies[4] and EPR calcite crystal measurements.[2] However, subsequent EPR studies of calcite crystals revealed the presence of both C_{2v} and D_{3h} structures for CO_3^-, thus indicating that the crystal environment might be responsible for the observed lower symmetry C_{2v} structure.[3] In addition, the authors of the matrix study of CO_3^- point out that NO_3^- (which most definitely has a D_{3h} structure) shows C_{2v} distortions in an argon matrix. Therefore, it seems that the experimental evidence cannot be considered to strongly favor either the C_{2v} or D_{3h} structures for CO_3^-. Therefore, for the purposes of calculating the electron affinity of CO_3 and thermodynamic quantities for CIMS reactions involving CO_3^-, we used the D_{3h} structure as the basis for the energy calculations.

While all of the symmetry breaking phenomenon observed for CO_3^- are also observed for CO_3 with respect to how the theoretical method influences the relative energies of the C_{2v} and D_{3h} structures, the fact that a C_{2v} stationary state for CO_3 is obtained from B3LYP geometry optimizations complicates making a definitive judgment about whether the CO_3 C_{2v} structure is an unphysical one. In addition, inspection of the MP2/6-31+G(d) harmonic vibrational frequencies obtained for the D_{3h} structure of CO_3 (Table 2), indicate an unphysically high value for one of the E′ states (although it should be pointed out that the B3LYP/6-31G+(d) harmonic vibrational frequency for that state is quite reasonable). Again, there is experimental evidence from IR matrix studies for a C_{2v} structure.[4,11,12] However, the same questions concerning the potential of the matrix environment to reduce the observed symmetry for CO_3^- apply to the case of CO_3 as well. Therefore, for purposes of calculating the electron affinity of CO_3, we used the D_{3h} structure as the basis for the energy calculations. Definitive structure optimization efforts involving the symmetry-constrained CASSCF/MRCI method described by Eisfeld and Morokuma,[24] will be required (and those are beyond the scope of the present work) to definitively address the structure question for CO_3 and CO_3^-. However, based on the near isoenergicity of the C_{2v} and D_{3h} states for the most sophisticated single reference electron correlation treatment (CCSD(T)), we will demonstrate that the choice of geometry for both CO_3 and CO_3^- does not significantly impact our energy calculations.

Electron affinity of CO_3

The electron affinity for CO_3 was calculated as a function of theoretical method (HF, MP2, CCSD, CCSD(T), CASSCF/MRCI) for the aug-cc-pVTZ basis set. The electron affinity was also calculated from the G2 and adapted G2MS model chemistry methods, with the geometry optimization steps constrained to a D_{3h} geometry for both CO_3 and CO_3^-. These results are presented in Table 4. It is apparent that the high level CCSD(T) and CASSCF/MRCI methods, as well as the CCSD(T)-extrapolated G2 and G2MS methods, result in very similar electron affinity values (ranging from 3.84 to 4.08 eV). The consistency of the single reference methods and the multireference CASSCF/MRCI method is not too surprising, given that the T_1 test[49] (from a CCSD(T)/6-31+G(d) calculation) for multireference character for CO_3 and CO_3^- yields values of 0.024 and 0.020, respectively. This result indicates modest multireference character for CO_3 and CO_3^- as compared to the large T_1 diagnostic (also determined from a CCSD(T)/6-31+G(d) calculation) of 0.117 for the highly multireference case of NO_3. To our knowledge, there have been no previous theoretical calculations performed for the electron affinity of CO_3. The experimental results for CO_3 electron affinity measurements are presented in Table 5.[6,7,26–31] Our results are in better agreement with the more recently obtained experimental values,[6,7,26] but our values are nonetheless somewhat higher than any of the experimental results. If electron affinities are calculated instead from all of the other possible C_{2v}

Table 4 Calculated CO_3 electron affinities (in eV)

Theoretical method	Electron affinity
HF/aug-cc-pVTZ	6.76
MP2/aug-cc-pVTZ	3.37
CCSD/aug-cc-pVTZ	4.88
CCSD(T)/aug-cc-pVTZ	4.08
CASSCF-MRCI/aug-cc-pVTZ	3.85
G2	3.91
G2MS	3.84

Table 5 Comparison of experimental CO_3 electron affinities (in eV)

Experimental method	Electron affinity	Ref.
Laser photoelectron spectroscopy	3.26 ± 0.17	7
From thermochemical cycle affinity and $\Delta_f H$	>3.34	6
From EA of radical/$\Delta_f H$ of anion	3.48 ± 0.18	26
Laser photoelectron spectroscopy	>3.0789	27
Ion–molecule reaction equilibrium	>2.7995	28
Photodetachment	2.69 ± 0.14	29
Photodetachment	3.25 ± 0.15	30
Collision induced dissociation threshold	3.10 ± 0.20	31

and D_{3h} geometry combinations for CO_3 and CO_3^- at the CCSD(T) level, the assumed D_{3h}–D_{3h} geometry case is actually the lowest electron affinity value calculated. Therefore, our relatively high values for the electron affinity cannot be attributed to the choice of reference geometry for energy calculations. For example, if a C_{2v} structure for CO_3 is assumed in the energy calculations, an electron affinity about 0.2 eV greater than for an assumed D_{3h} geometry is calculated. Thus, any uncertainty about the choice of structures for CO_3 and CO_3^- exerts a relatively small influence on the calculated electron affinity.

Thermodynamics validation calculations

These calculations (compiled in Table 6) show that the accuracy of the G2MS method is about 0.1 eV compared to literature values, which is about the same as that of the G2 method (0.1 eV) for these molecules.[34] In particular, if only the ion–molecule reactions $O_2^- + H_2O \rightarrow O_2^-(H_2O)$ and $CO_3^- + H_2O \rightarrow CO_3^-(H_2O)$ are considered, which are similar to chemical ionization reactions under tudy here, the accuracy is seen to be even greater. Therefore, it can be seen that the G2MS method performs at least as well as the G2 method for these molecules, with a significant savings in computational resources over the G2 method. However, it is necessary to use at least the G2MS level because lower levels of theory do not give sufficiently accurate results. For example, we have determined that the standard deviation from experimental values for the MP2/6-31G(d) level is 0.7 eV and at the MP2/6-311+G(d,p) level is 0.3 eV.[34]

Evaluation of potential CIMS detection scheme

Because ion–molecule reactions often proceed near the collision-limited rate, thermodynamic data are often predictive of suitable chemical ionization schemes [*i.e.*, exoergic ($\Delta G < 0$) reactions proceed rapidly].[50] The optimized geometry, enthalpy and Gibbs energy for each of the involved species were calculated and ΔH and ΔG for the H_2O_2 reactions below were calculated to determine their thermodynamic feasibility:

$$CO_3^- + H_2O_2 \rightarrow CO_3^-(H_2O_2) \quad (4)$$

$$CO_3^- + H_2O_2 \rightarrow O_2^- + CO_2 + H_2O \quad (5)$$

$$CO_3^-(H_2O) + H_2O_2 \rightarrow CO_3^-(H_2O_2) + H_2O \quad (6)$$

$$CO_3^-(H_2O) + H_2O_2 \rightarrow O_2^-(H_2O) + CO_2 + H_2O \quad (7)$$

ΔH and ΔG were similarly calculated for the CH_3OOH reactions below:

$$CO_3^- + CH_3OOH \rightarrow CO_3^-(CH_3OOH) \quad (8)$$

$$CO_3^- + CH_3OOH \rightarrow O_2^- + CH_3OH + CO_2 \quad (9)$$

$$CO_3^- + CH_3OOH \rightarrow O_2^-(CH_3OH) + CO_2 \quad (10)$$

$$CO_3^-(H_2O) + CH_3OOH \rightarrow CO_3^-(CH_3OOH) + H_2O \quad (11)$$

$$CO_3^-(H_2O) + CH_3OOH \rightarrow O_2^-(H_2O) + CH_3OH + CO_2 \quad (12)$$

The calculated structures of all species are given in Fig. 4–6, Tables 7 and 8 or listed below and were determined *via* geometry optimization at the B3LYP/6-31+G(d,p) level, unless otherwise noted. CO_2 was calculated to have a linear geometry with the two C–O bonds lengths determined to be 1.169 Å. H_2O was calculated to have an H–O–H bond angle of 105.75° and the two O–H bonds were determined to be 0.965 Å. Hydrogen peroxide was found to have the following structural parameters: O–H bond lengths of 0.971 Å, O–O bond length of 1.457 Å, H–O–O bond angles of 100.3° and a H–O–O–H dihedral angle of 119.5°. The values are in good agreement with the experimentally determined structures.[51] O_2^- was calculated to have a O–O bond length of 1.296 Å. The harmonic vibrational frequencies (calculated at the B3LYP/6-31+G(d,p) level) are given in Table 9.

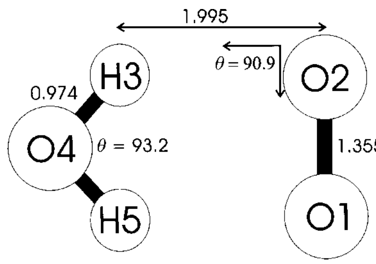

Fig. 4 The ground state geometry for $O_2^-(H_2O)$ calculated at the B3LYP/6-31+G(d,p) level. The molecule has a planar C_{2v} structure. All angles are in degrees and bond lengths in Å.

It can be seen that for all of the CO_3^- complexes formed, CO_3^- tends to bond in a bidentate manner, thus the CO_3^- subunit often assumes local C_{2v} or C_s symmetry (and symmetry breaking effects are therefore not relevant in the CO_3^- complexes). In our previous calculations on the feasibility of CIMS detection of peroxides with the $F^-(H_2O)_n$ reagent ion, we found a similar bidentate bonding between F^- and H_2O_2 and F^- and CH_3OOH,[34] although the C–H–F bond formed in the CH_3OOH complex was found to be much weaker than the second (O–H–F) bond formed in the CH_3OOH complex

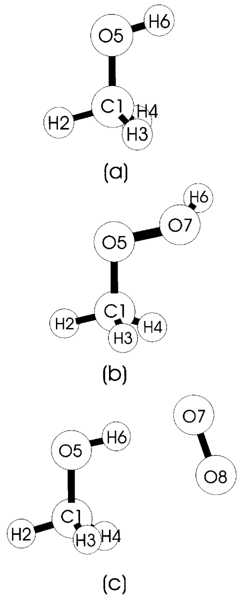

Fig. 5 The ground state geometries calculated for (a) CH_3OH, (b) CH_3OOH and (c) $O_2^-(CH_3OH)$ at the B3LYP/6-31+G(d,p) level. The geometrical parameters are given in Table 7.

Table 6 Validation calculations of ionic standard thermodynamic values (in eV)

	MP2/ 6-31G(d)[34]	MP2/ 6-311+G(d,p)[34]	G2[34]	G2MS	Exp.
Ionisation potential (O_2)	11.55	11.51	12.17	11.96	12.06[52]
Electron affinity (NO_2)	1.03	1.89	2.34	2.18	2.27[53]
Proton affinity (H_2O)	7.20	7.10	7.07	7.06	7.16[54]
Fluoride affinity (HCl)	4.09	2.52	2.54	2.68	2.53[54]
ΔH [$O_2^- + H_2O \rightarrow O_2^-(H_2O)$]	−1.25	−0.92		−0.82	−0.80[55]
ΔH [$CO_3^- + H_2O \rightarrow CO_3^-(H_2O)$]	−0.05	−0.13		−0.56	−0.61[55]

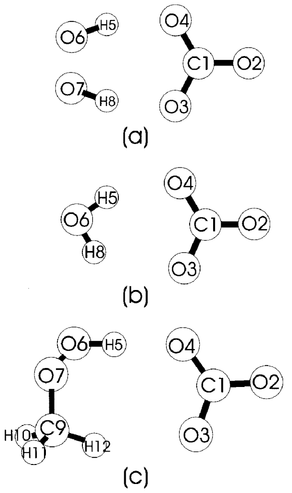

Fig. 6 The ground state geometries calculated for (a) $CO_3^-(H_2O_2)$, (b) $CO_3^-(H_2O)$ and (c) $CO_3^-(CH_3OOH)$ at the B3LYP/6-31+G(d,p) level. The geometrical parameters are given in Table 8.

or the identical O–H–F bonds formed in the H_2O_2 complex. For both H_2O_2 and CH_3OOH, upon formation of a complex with CO_3^-, the C1–O2 bond not involved in bonding lengthens while the C1–O3 and C1–O4 bonds involved in bonding shorten. For $CO_3^-(H_2O_2)$, CO_3^- assumes a local C_{2v} geometry, however it is unlike the C_{2v} structure discussed for the bare ion because the unique angle is greater (123.7°) than 120° in the complex rather than smaller than 120°. For both $CO_3^-(H_2O)$ and $CO_3^-(CH_3OOH)$, CO_3^- adopts a local C_s geometry where none of the O–C–O bonds angles are equal nor are any of the C–O bond lengths.

Table 10 shows the calculated standard enthalpy and Gibbs energy of reaction for reactions (4)–(7) and (8)–(12). It can be seen that all of the reactions involving H_2O_2 are thermodynamically feasible (exoergic, ($\Delta G < 0$). It is worth noting that the complications (due to symmetry breaking effects) in the choice of geometry for the energy calculations for the bare CO_3^- ion do not influence the value of ΔG calculated for reactions (4), (5) and (8)–(10). If a C_{2v} geometry is assumed for CO_3^- for the energy calculations, the calculated thermodynamic values are only about 0.1 eV different than for energies calculated for an assumed D_{3h} structure, and in no case is the sign of ΔG or ΔH changed. In particular, both reactions (5) and (7) are entropically favored, and in the case of reaction (5) this increase in entropy increases the exoergicity of the reaction from 0.10 to −0.27 eV. In other words, the entropy term is responsible for increasing the exoergicity such that the reaction is predicted to be thermodynamically spontaneous. On the other hand, reactions (4) and (6) are entropically disfavored. Despite this decrease in entropy, both reactions (4) and (6) remain exoergic. Therefore, we predict that it is possible to use both CO_3^- and $CO_3^-(H_2O)$ as the reagent ion in CIMS to detect H_2O_2 *via* reactions (4)–(7). Thus, in principle, H_2O_2 could be detected by $CO_3^-(H_2O)_n$ CIMS by monitoring at $m/z = 94$ ($CO_3^-(H_2O_2)$), 50 ($O_2^-(H_2O)$) or 32 (O_2^-) u. Since this result indicates that it is possible to detect hydrogen peroxide at three different viable masses using CIMS, this approach may be beneficial in dealing with potential interferences from the other chemical species that may arise during *in situ* measurements.

Table 7 Geometrical parameters for CH_3OOH, CH_3OH and $O_2^-(CH_3OH)$ calculated at the B3LYP/6-31+G(d,p) level. Bond lengths are given in Å and angles in degrees. Atom labels are given in Fig. 4

Bond length	CH_3OH	CH_3OOH	$O_2^-(CH_3OH)$
C1–H2	1.093	1.095	1.094
C1–H3	1.101	1.096	1.092
C1–H4	1.101	1.098	1.094
C1–O5	1.419	1.417	1.416
O5–H6	0.965		0.998
O5–O7		1.457	
O7–H6		0.971	
H6–O7			1.701
O7–O8			1.339
Bond angle			
H2–C1–H3	107.9	109.6	109.3
H2–C1–H4	107.9	109.7	108.7
H2–C1–O5	106.9	104.6	107.5
C1–O5–H6	107.6		107.5
C1–O5–O7		106.1	
O5–O7–H6		99.8	
O5–H6–O7			178.4
H6–O7–O8			96.0
Dihedral angle			
H2–C1–O5–H6	108		176.2
H3–C2–O5–H6	61.5		56.3
H4–C1–O5–H6	−615		−64.4
H2–C1–O5–O7		177.2	
H3–C1–O5–O7		58.9	
H4–C1–O5–O7		−64.1	
C1–O5–O7–H6		115.2	
C1–O5–H6–O7			−6.1
O5–H6–O7–O8			0.8

Table 8 Geometric parameters of associations formed between CO_3^- and H_2O, H_2O_2 and CH_3OOH calculated at the B3LYP/6-31+G(d,p) level. Bond lengths are given in Å and angles in degrees. Atom labels are given in Fig. 5

Bond length	$CO_3^-(HOOH)$	$CO_3^-(H_2O)$	$CO_3^-(CH_3OOH)$
C1–O2	1.288	1.286	1.287
C1–O3	1.273	1.279	1.282
C1–O4	1.273	1.269	1.264
O4–H5	1.801	1.961	1.689
H5–O6	0.991	0.979	1.003
O6–O7	1.459		1.453
O6–H8		0.969	
O7–H8	0.991		
O7–C9			1.421
C9–H10			1.098
C9–H11			1.01
C9–H12			1.096
Bond angle			
O2–C1–O3	118.2	116.7	114.0
O3–C1–O4	123.7	122.8	123.8
C1–O4–H5	113.1	110.3	126.2
O4–H5–O6	162.9	154.2	175.1
H5–O6–O7	101.6		102.1
H5–O6–H8		99.3	
O6–O7–H8	101.6		
O6–O7–C9			107.0
O7–C9–H10			104.8
O7–C9–H11			110.8
O7–C9–H12			111.3
Dihedral angle			
O4–C1–O2–O3	180	180	−179.9
H5–O4–C1–O3	7.2	0	8.6
H5–O6–O7–H8	42.4		
O4–H5–O6–H8	−30.2	0	
H5–O6–O7–C9			86.7
O6–O7–C9–H10			60.5
O6–O7–C9–H11			178.7
O6–O7–C9–H12			−62.6

It can be seen in Table 7 that reactions (8), (10), (11) and (12), involving CH_3OOH, were found to be thermodynamically favored whereas reaction (9) is not favored. As with the H_2O_2 calculations above, reactions (9) and (12) are entropically favored. However, this difference provided by entropy is not enough to make reaction (9) exoergic as well ($\Delta G = 0.07$ eV). Thus, reaction (9) is not predicted to be thermodynamically feasible (although within the estimated error of the computation technique, it is possible that $\Delta G < 0$) whereas

Table 9 Harmonic frequencies (in cm^{-1}, calculated at the B3LYP/6-31G+(d,p) level) for various species used in thermodynamic calculations

Species	Frequencies
H_2O	1603, 3809, 3931
CO_2	640, 640, 1372, 2436
H_2O_2	372, 946, 1301, 1445, 3770, 3771
CH_3OH	330, 1060, 1094, 1179, 1385, 1499, 1509, 1526, 2989, 3035, 3122, 3830
CH_3OOH	187, 254, 447, 888, 1050, 1177, 1212, 1371, 1460, 1475, 1527, 3017, 3089, 3125, 3756
O_2^-	1173
$O_2^-(H_2O)$	245, 280, 419, 485, 789, 1081, 1738, 3709, 3855
$O_2^-(CH_3OH)$	24, 69, 102, 204, 295, 1002, 1100, 1162, 1177, 1192, 1469, 1490, 1506, 1603, 2664, 2948, 2976, 2995
$CO_3^-(H_2O)$	39, 91, 188, 329, 392, 401, 625, 731, 794, 935, 1336, 1704, 1710, 3748, 3797
$CO_3^-(H_2O_2)$	47, 99, 140, 189, 223, 343, 505, 637, 671, 812, 942, 1086, 1252, 1418, 1495, 1544, 3341, 3388
$CO_3^-(CH_3OOH)$	21, 46, 70, 91, 136, 207, 286, 383, 450, 512, 809, 868, 884, 1044, 1094, 1178, 1201, 1215, 1447, 1470, 1476 1517, 1539, 2993, 3069, 3100, 3162

Table 10 The calculated standard thermodynamic values (in eV) for reactions between H_2O_2 and CH_3OOH with CO_3^- and $CO_3^-(H_2O)$ using G2MS theory

Reaction		ΔH	ΔG
$CO_3^- + H_2O_2 \rightarrow CO_3^-(H_2O_2)$	(4)	−0.89	−0.49
$CO_3^- + H_2O_2 \rightarrow O_2^- + CO_2 + H_2O$	(5)	0.10	−0.27
$CO_3^-(H_2O) + H_2O_2 \rightarrow CO_3^-(H_2O_2) + H_2O$	(6)	−0.35	−0.24
$CO_3^-(H_2O) + H_2O_2 \rightarrow O_2^-(H_2O) + CO_2 + H_2O$	(7)	−0.18	−0.48
$CO_3^- + CH_3OOH \rightarrow CO_3^-(CH_3OOH)$	(8)	−0.71	−0.35
$CO_3^- + CH_3OOH \rightarrow O_2^- + CH_3OH + CO_2$	(9)	0.45	0.07
$CO_3^- + CH_3OOH \rightarrow O_2^-(CH_3OH) + CO_2$	(10)	−0.57	−0.65
$CO_3^-(H_2O) + CH_3OOH \rightarrow CO_3^-(CH_3OOH) + H_2O$	(11)	−0.18	−0.09
$CO_3^-(H_2O) + CH_3OOH \rightarrow O_2^-(H_2O) + CH_3OH + CO_2$	(12)	0.17	−0.15

reaction (12) is predicted to be exoergic ($\Delta G = -0.15$ eV). Reaction (17) is entropically disfavored, yet this decrease in entropy is small enough such that the Gibbs energy change remains negative. The Gibbs energy change for reaction (11) is negative ($\Delta G = -0.09$ eV) but the error on these calculations is large enough to make this result uncertain. Thus, we predict that CH_3OOH can be detected using CO_3^- or $CO_3^-(H_2O)$ as the reagent ion *via* CIMS. CH_3OOH could potentially be detected by $CO_3^-(H_2O)_n$ CIMS by monitoring at $m/z = 108$ ($CO_3^-(CH_3OOH)$, 64 ($O_2^-(CH_3OH)$) or 50 ($O_2^-(H_2O)$) u. Note, however, that $CO_3^-(H_2O)$ is predicted to react with both H_2O_2 and CH_3OOH to produce $O_2^-(H_2O)$ ($m/z = 50$ u). Therefore this reaction is a potential interference process for the unique detection of these peroxides. Reiner *et al.* have identified ions at 94 u ($CO_3^-(H_2O_2)$) and 50 u ($O_2^-(H_2O)$) from the reaction of $CO_3^-(H_2O)$ with H_2O_2 in a laboratory study. Reiner *et al.* have observed a CIMS signal at $m/z = 94$ amu using $CO_3^-(H_2O)$ as the reagent ion during *in situ* measurements made in the lower stratosphere and have tentatively identified this signal as due to $CO_3^-(H_2O_2)$ resulting from reaction (6).[33] Therefore, our computational results suggest that a $CO_3^-(H_2O)$ CIMS detection scheme may be a general method for the unique observation of ROOH species, as the $CO_3^-(H_2O)$ reactions in which the parent mass is conserved in the ion are predicted to be thermodynamically accessible for both H_2O_2 and CH_3OOH:

$$CO_3^-(H_2O) + ROOH \rightarrow CO_3^-(ROOH) + H_2O \quad (13)$$

Conclusions

Electronic structure calculations have shown that both CO_3 and CO_3^- are prone to be influenced by symmetry breaking effects, which we find are likely to lead to the C_{2v} potential energy minima observed with most of the theoretical methods employed in this work. Therefore, because of this artifactual bias towards the C_{2v} structures for CO_3 and CO_3^-, we believe that D_{3h} structures are in fact the only physical potential energy minima for these molecules. Definitive conclusions concerning the equilibrium structures of CO_3 and CO_3^- will have to await the completion of symmetry-constrained CASSCF/MRCI optimization studies similar to those described by Eisfeld and Morokuma for NO_3.[24]

The first computational estimates for the electron affinity of CO_3 (calculated for D_{3h} structures for both the neutral and the anion) have been performed using the high level single reference CCSD(T)/aug-cc-pVTZ, G2, and G2MS theories and the multireference CASSCF/MRCI (aug-cc-pVTZ basis) method. The computational results from these methods are fairly consistent, with values ranging from 3.84 to 4.08 eV. These values are somewhat higher than the more recent experimental electron affinity measurements which report values of about 3.5 eV.[6,7,26]

Our results indicate that there is thermodynamic support for using CO_3^- and $CO_3^-(H_2O)$ as reagent ions in CIMS detection schemes for both H_2O_2 and CH_3OOH. Reiner *et al.* have shown experimentally that H_2O_2 can indeed be detected using CIMS with $CO_3^-(H_2O)$ as the reagent ion.[33] Therefore, we propose that $CO_3^-(H_2O)$ CIMS could potentially be extended as a general detection method for ROOH species.

Acknowledgements

The authors acknowledge support from the National Science Foundation (ATM9874752), the Camille and Henry Dreyfus Foundation and the Towsley Foundation.

References

1 F. Arnold, *Atmospheric Chemistry*, Springer, New York, 1982.
2 G. W. Chantry, A. Horsfield, J. R. Morton and D. H. Whiffen, *Mol. Phys.*, 1962, **5**, 589.

3 R. A. Serway and S. A. Marshall, *J. Chem. Phys.*, 1967, **47**, 868.
4 M. E. Jacox and D. E. Milligan, *J. Mol. Spectrosc.*, 1974, **52**, 363.
5 J. T. Moseley, P. C. Cosby and J. R. Peterson, *J. Chem. Phys.*, 1976, **65**, 2512.
6 D. E. Hunton, M. Hofmann, T. G. Lindeman and A. W. Castleman and Jr., *J. Chem. Phys.*, 1985, **82**, 134.
7 J. T. Snodgrass, C. M. Roehl, A. M. van Koppen, W. E. Palke and M. T. Bowers, *J. Chem. Phys.*, 1990, **92**, 5935.
8 J. F. Olsen and L. Burnelle, *J. Am. Chem. Soc.*, 1970, **92**, 3659.
9 S. P. So, *J. Chem. Soc.*, *Faraday Trans. 2*, 1976, **72**, 646.
10 R. D. J. Froese and J. D. Goddard, *J. Phys. Chem.*, 1993, **97**, 7484.
11 N. G. Moll, D. R. Clutter and W. E. Thompson, *J. Chem. Phys.*, 1966, **45**, 4469.
12 E. Weissberger, W. H. Breckenridge and H. Taube, *J. Chem. Phys.*, 1967, **47**, 1764.
13 M. E. Jacox and D. E. Milligan, *J. Chem. Phys.*, 1971, **54**, 919.
14 B. J. Gimarc and T. S. Chou, *J. Chem. Phys.*, 1968, **49**, 4043.
15 J. A. Pople, U. Seeger, R. Seeger and P. v. R. Schleyer, *J. Comput. Chem.*, 1980, **1**, 199.
16 M. Cornille and J. Horsely, *Chem. Phys. Lett.*, 1970, **6**, 373.
17 J. R. Sabin and H. Kim, *Chem. Phys. Lett.*, 1971, **11**, 593.
18 P. LaBonville, R. Kugel and J. R. Ferraro, *J. Chem. Phys.*, 1977, **67**, 1477.
19 J. A. Tossell, *Physica B*, 1985, **131**, 283.
20 J. S. Francisco and I. H. Williams, *Chem. Phys.*, 1985, **95**, 373.
21 W. J. Van De Guchte, J. P. Zwart and J. J. C. Mulder, *J. Mol. Struct.*, 1987, **152**, 213.
22 S. Canuto and G. H. F. Diercksen, *Chem. Phys.*, 1988, **120**, 375.
23 M. A. Castro and S. Canuto, *Chem. Phys. Lett.*, 1991, **177**, 98.
24 W. Eisfeld and K. Morokuma, *J. Chem. Phys.*, 2000, **113**, 5587.
25 C. E. Miller and J. S. Francisco, *J. Phys. Chem. A*, 2001, **105**, 1662.
26 J. F. Hiller and M. L. Vestal, *J. Chem. Phys.*, 1980, **72**, 4713.
27 S. E. Novich, P. C. Engelking, P. L. Jones, J. H. Futrell and W. C. Lineberger, *J. Chem. Phys.*, 1979, **70**, 2652.
28 I. Dotan, J. A. Davidson, G. E. Streit, D. L. Albritton and F. C. Fehsenfeld, *J. Chem. Phys.*, 1977, **67**, 2874.
29 S. P. Hong, S. B. Woo and E. M. Helmy, *Phys. Rev. A*, 1977, **15**, 1563.
30 M. L. Vestal and G. H. Mauclaire, *J. Chem. Phys.*, 1977, **67**, 3758.
31 T. O. Tiernan and R. L. C. Wu, *Adv. Mass Spectrom, Part. A*, 1978, **7**, 136.
32 B. J. Finlayson-Pitts and J. N. Pitts, *Chemistry of the Upper and Lower Atmosphere*, Academic Press, San Diego, 2000.
33 T. Reiner, O. Mohler and F. Arnold, *J. Geophys. Res.*, 1998, **103**, 31309.
34 B. M. Messer, D. E. Stielstra, C. D. Cappa, K. W. Scholtens and M. J. Elrod, *Int. J. Mass Spectrom.*, 2000, **197**, 219.
35 M. J. Elrod, D. L. Ranschaert and N. J. Schneider, *Int. J. Chem. Kinet.*, 2001, **33**, 363.
36 A. D. Becke, *J. Chem. Phys.*, 1993, **98**, 5648.
37 G. D. Purvis and R. J. Bartlett, *J. Chem. Phys.*, 1982, **76**, 1910.
38 K. Raghavachari, G. W. Trucks, J. A. Pople and M. Head-Gordon, *Chem. Phys. Lett.*, 1989, **157**, 479.
39 M. J. Frisch, G. W. Trucks, H. B. Schlegel, G. E. Scuseria, M. A. Robb, J. R. Cheeseman, V. G. Zakrzewski, Jr., J. A. Montgomery, R. E. Stratmann, J. C. Burant, S. Dapprich, J. M. Millam, A. D. Daniels, K. N. Kudin, M. C. Strain, O. Farkas, J. Tomasi, V. Barone, M. Cossi, R. Cammi, B. Mennucci, C. Pomelli, C. Adamo, S. Clifford, J. Ochterski, G. A. Petersson, P. Y. Ayala, Q. Cui, K. Morokuma, K. K. Malick, A. D. Rabuck, K. Raghavachari, J. B. Foresman, J. Cioslowski, J. V. Ortiz, A. G. Baboul, B. B. Stefanov, G. Liu, A. Liashenko, P. Piskorz, I. Komaromi, R. Gomperts, R. L. Martin, D. J. Fox, T. Keith, M. A. Al-Laham, C. Y. Peng, A. Nanayakkara, C. Gonzalez, M. Challacombe, P. M. W. Gill, B. Johnson, W. Chen, M. W. Wong, J. L. Andres, C. Gonzalez, M. Head-Gordon, E. S. Replogle and J. A. Pople, Gaussian98, v.A7, Inc., Pittsburgh, PA, 1998.
40 B. O. Roos, in *Methods in Computational Molecular Physics*, ed. G. H. F. Diercksen and S. Wilson, Reidel, Dordrecht, 1983, pp. 161–187.
41 H.-J. Werner and P. J. Knowles, *J. Chem. Phys.*, 1988, **89**, 5803.
42 *MOLPRO* is a package of *Ab Initio* programs written by H.-J. Werner and P. J. Knowles with contributions from J. Almlof, R. D. Amos, A. Berning, L. D. Cooper, M. J. O. Deegan, A. J. Dobbyn, F. Eckert, S. T. Elbert, C. Hampel, R. Lindh, A. W. Lloyd, W. Meyer, A. Nicklass, K. Peterson, R. Pitzer, A. J. Stone, P. R. Taylor, M. E. Mura, P. Pulay, M. Schutz, H. Stoll and T. Thorsteinsson.
43 A. Wilson, A. Van Mourik and T. H. Dunning, Jr., *J. Mol. Struct.* (*Theochem*), 1997, **388**, 339.
44 R. D. J. Froese, S. Humbel, M. Svensson and K. Morokuma, *J. Phys. Chem. A*, 1997, **101**, 227.
45 L. A. Curtiss, K. Raghavachari, G. W. Trucks and J. A. Pople, *J. Chem. Phys.*, 1991, **94**, 7221.
46 R. D. Davy and H. F. Schaefer III, *J. Chem. Phys.*, 1989, **91**, 4410.
47 L. A. Eriksson, J. Wang, R. J. Boyd and S. Lunell, *J. Phys. Chem.*, 1994, **98**, 792.
48 C. D. Sherrill, M. S. Lee and M. Head-Gordon, *Chem. Phys. Lett.*, 1999, **302**, 425.
49 T. J. Lee and P. R. Taylor, *Int. J. Quantum Chem.*, *Quantum Chem. Symp.*, 1989, **23**, 199.
50 M. T. Bowers, *Gas Phase Ion Chemistry*, Academic Press, New York, 1979.
51 G. Herzberg, *Electronic Spectra of Polyatomic Molecules*, Van Nostrand, Princeton, NJ, 1967.
52 R. G. Tonkyn, J. W. Winniczek and M. G. White, *Chem. Phys. Lett.*, 1989, **164**, 137.
53 K. M. Ervin, J. Ho and W. C. Lineberger, *J. Phys. Chem.*, 1988, **92**, 5405.
54 E. P. Hunter and S. G. Lias, *J. Phys. Chem. Ref. Data*, 1998, **27**.
55 R. G. Keesee and A. W. Castleman, *J. Phys. Chem. Ref. Data*, 1986, **15**, 1011.